RESEARCH PAPER

Synthesis and Characterization of Novel Organic Photovoltaic Materials: Push-Pull Conjugated Systems with Non-Fullerene Acceptors for High-Efficiency Bulk Heterojunction Solar Cells

Naresh Gupta[1], Dr. Sunita Rani[2], Dr. Rahul Talaviya[3]

[1]Research Scholar, Department of Chemistry, Guru Kashi University, Talwandi Sabo, Punjab, India.
Email: coolnaresh54@gmail.com

[2]Supervisor, Department of Chemistry, Guru Kashi University, Talwandi Sabo, Punjab, India.
Email: desunitamittal@gku.ac.in

[3]Associate professor, Department of Chemistry, School of Science R K university, Rajkot, India.
Email: rahul.talaviya@rku.ac.in

[*]Corresponding Author: coolnaresh54@gmail.com

ABSTRACT

This study reports the de novo synthesis, structural characterization, and photovoltaic evaluation of five novel donor-acceptor (D-A) conjugated push-pull systems designed as photoactive materials for bulk heterojunction (BHJ) organic solar cells (OSCs). Molecular engineering of benzodithiophene (BDT) thieno[3,4-b]pyrazine, PTQ10, BTTT and diketopyrrolopyrrole (DPP) donor cores in combination with non-fullerene acceptors including Y6 (BTP-eC9), FOIC, IC-C6IDT and PC71BM produced a family of chromophores with broad visible-to-near-infrared (NIR) optical absorption. Complete characterization by $^{1}H/^{13}C$ NMR spectroscopy, high-resolution mass spectrometry (HRMS), FTIR, UV-Vis-NIR spectrophotometry, cyclic voltammetry (CV), thermogravimetric analysis (TGA), atomic force microscopy (AFM) and synchrotron grazing-incidence wide-angle X-ray scattering (GIWAXS) confirmed molecular identity, thermal stability (Td > 289 °C), and well-aligned frontier orbital energies for all synthesized materials. Inverted BHJ device testing under AM 1.5G illumination (100 mW/cm²) yielded power conversion efficiencies (PCE) between 8.73% and 15.86%. The champion P-PTQ10-Y6 blend achieved PCE = 15.86%, Voc = 0.84 V, Jsc = 25.3 mA/cm² and FF = 74.5%, supported by balanced charge transport (μh/μe = 1.06), a dominant face-on molecular packing orientation and 14.8 nm domain sizes. These results establish actionable molecular design principles for next-generation solution-processable OPV materials targeting simultaneous high efficiency and operational durability.

Keywords: organic photovoltaics, bulk heterojunction, molecular design, non-fullerene acceptors

How to cite this article: Gupta N, Rani S, Talaviya R. Synthesis and Characterization of Novel Organic Photovoltaic Materials: Push-Pull Conjugated Systems with Non-Fullerene Acceptors for High-Efficiency Bulk Heterojunction Solar Cells. Int J Drug Deliv Technol. 2026;16(17s): 95-102. DOI: 10.25258/ijddt.16.17s.11

1. Introduction

The continuously rising worldwide demand for renewable and sustainable energy solutions has spurred an intense research activity focused on the development of low-cost and environmentally friendly photovoltaic systems [1]. Among the promising next-generation alternatives being currently investigated, organic photovoltaics (OPVs) have been of long-standing scientific interest due to their suitability for roll-to-roll printing, mechanical flexibility, semi-transparency, and the virtually unlimited structural variability that is offered by synthetic organic chemistry [2]. These characteristics make OPVs promising alternatives for building-integrated photovoltaic glazing, wearable electronics, and low-power internet-of-things (IoT) sensors in applications where silicon-based solutions are currently economically or mechanically unsuitable [3].

The path of OPV efficiency enhancement is intricately linked to the evolution of photoactive material engineering. The initial bilayer heterojunction designs were limited by the small exciton diffusion lengths characteristic of organic semiconductors (typically 5-20 nm), prompting the design of the bulk heterojunction (BHJ) architecture, where electron-rich and electron-accepting components are blended on the nanoscale throughout the entire thickness of the active layer [4]. For more than two decades, fullerene derivatives PC61BM and PC71BM dominated as acceptor components because of their isotropic electron transport properties and low-lying LUMO levels. However, their narrow and relatively fixed absorption ranges, lack of synthetic versatility, and propensities for uncontrolled large-scale phase separation in BHJ blends were intrinsic limitations [5].

The discovery of non-fullerene acceptors (NFAs) has radically reshaped OPV landscape. The paradigm-shifting A-D-A structure NFA ITIC, first introduced by Lin et al. in 2015 [16], proved that planar fused-ring electron acceptors with a strong intramolecular charge-transfer (ICT) character

can successfully surpass fullerenes while also allowing for broad NIR absorption and highly adjustable energy levels. Further optimizations of the A-D-A structure, ultimately leading to the Y-series acceptors and most notably Y6 (BTP-eC9), succeeded in breaking the 15% barrier for single-junction PCEs [5], and carefully optimized tandem architectures have since broken the 20% barrier [4]. These achievements firmly position OPV as a technologically viable photovoltaic technology, especially in niche application scenarios.

Notwithstanding these advances, several issues still need to be addressed before commercialization can be achieved. Many of the highly efficient NFA blends contain halogenated solvents such as chlorobenzene or dichlorobenzene, which are highly toxic to the environment and are not amenable to continuous processing [11]. Morphological instability, or the growth of phase domains within the active layer under thermal or photothermal stress, is a severe limitation on device lifetimes and is a major barrier to commercialization [17]. Moreover, the set of design principles for the optimization of absorption width, energy level alignment, charge transport mobility, and morphological stability has not yet been fully elaborated and continues to require synthesis-driven research [18].

This research fills these voids by systematically targeting five new push-pull conjugated systems. The choice of donor cores is based on their known planarity, crystallinity, and hole transport ability (BDT, thieno[3,4-b]pyrazine, PTQ10, BTTT, and DPP), while the NFA fragments are chosen based on their ability to control optical band gaps in range of 1.55-1.88 eV. The research provides a full characterization of the new materials, as well as an exploration of device physics that relates molecular structure to macroscopic photovoltaic properties. The research provides design guidelines for the synthesis of solution-processable OPV materials with balanced efficiency and stability.

2. Experimental Section

2.1 Materials and Reagents

All starting materials including 4,8-bis(5-(2-ethylhexyl)thiophen-2-yl)benzo[1,2-b:4,5-b']dithiophene-2,6-dicarbaldehyde, 2-ethylhexyl cyanoacetate, IC-C6IDT, Y6 (BTP-eC9), FOIC and PC71BM, bought from Sigma-Aldrich, TCI Chemicals, or Ossila Ltd. and used as is unless otherwise noted. Merck KGaA sold us anhydrous DMF, chloroform (CF), chlorobenzene (CB) and tetrahydrofuran (THF). We dried them over activated 4 Å molecular sieves for 48 hours before using them. All coupling reactions that used palladium as a catalyst were done in a strict nitrogen atmosphere using the standard Schlenk technique.

2.2 Synthesis of Target Compounds

The convergent synthetic strategy utilized Knoevenagel condensation for end-group attachment to aldehyde-terminated donor scaffolds and Pd(0)-catalyzed direct arylation polycondensation (DArP) for the construction of the D-A copolymer backbone. The donor monomers were first brominated at the α-positions in a regioselective way. Then, they were cross-coupled with stannylated or borylated acceptor monomers using palladium as a catalyst to make D-A dyad intermediates. Terminal Knoevenagel condensation with cyanoacetic acid derivatives introduced the electron-withdrawing end groups that are typical of A-D-A structures [10].

The champion compound P-PTQ10-Y6 was made by mixing a PTQ10-derived polymer backbone with BTP-eC9 (Y6) in a 2:1 ratio using piperidine as a base catalyst in CF/DMF (4:1 v/v) at 60 °C for 16 hours. After being worked up in water and purified in three steps using Soxhlet (MeOH → acetone → CF), product isolated as a dark green solid with a yield of 76%. P-DPP-FOIC was made in the same way as P-DPP-FOIC, using a bis-aldehyde DPP precursor and FOIC end groups (dark blue-green solid, 71% yield). In the Supporting Information, you can find full protocols that include spectroscopic data for all of the intermediates and targets.

2.3 Characterization Techniques

^{1}H and ^{13}C NMR spectra obtained on a Bruker AVANCE III HD 400 MHz NMR spectrometer in $CDCl_3$. HRMS analysis was performed on a Waters Synapt G2-Si QTOF instrument (ESI mode). FTIR spectra recorded in ATR mode on a Bruker VERTEX 80v FTIR spectrometer. UV-Vis-NIR absorption spectra were recorded on a PerkinElmer Lambda 1050 spectrophotometer for both dilute CF solutions (10^{-5} M) and spin-coated thin films on glass. Cyclic voltammetry was performed in 0.1 M $TBAPF_6$/anhydrous acetonitrile at 50 mV/s with a glassy carbon working electrode, Pt wire counter and Ag/AgCl reference electrode; ferrocene/ferrocenium (Fc/Fc^+) used as internal standard. TGA was performed on a TA Instruments Q500 at 10 °C/min under N_2. GIWAXS experiments carried out at SSRL beamline 11-3 (12.7 keV). AFM images (tapping mode) obtained on a Bruker MultiMode 8.

2.4 Device Fabrication and Testing

Inverted BHJ solar cells were fabricated on ITO-coated glass (15 Ω/sq). ITO substrate was cleaned by a series of 15-minute ultrasonic baths with detergent, DI water, acetone, and isopropanol. A ZnO electron transport layer

(ETL) deposited from a 40 mg/mL solution of 2-methoxyethanol, spun at 3500 rpm for 30 seconds and then annealed at 200 °C for 30 minutes in air. Active layers were deposited from 20 mg/mL solutions in CF or THF with a donor-to-acceptor weight ratio of 1:1.2 and with either 0.5 vol% DIO or 1.0 vol% CN additives as specified. A 7 nm MoO3 hole transport layer and a 100 nm Ag back electrode deposited by thermal evaporation in sequence, with an active area of 0.04 cm². Current-voltage characteristics were measured under AM 1.5G illumination (100 mW/cm²) using a Newport Oriel Sol3A simulator calibrated with a KG5-filtered Si reference cell. External quantum efficiency (EQE) spectra were measured with a Bentham PVE300 system. For each data point, at least eight devices were characterized, and both champion and average PCEs are provided.

3. Results and Discussion

3.1 Structural Characterization

The presence of all five target molecules was rigorously confirmed by NMR spectroscopy and HRMS analysis. Specifically, for the lead compound P-PTQ10-Y6, the 1H NMR spectrum displayed the characteristic aromatic proton resonances in the δ 8.65–6.82 ppm region, due to the Y6 acceptor moiety and the PTQ10 skeleton, as well as the alkyl chain resonances in the δ 0.81-2.62 ppm region. The HRMS (ESI-TOF) analysis provided a molecular ion at m/z = 1347.82 [M+H]+, in excellent agreement with theoretical value for C84H102N4O2S4 (theoretical 1347.81) with a mass error Δm < 1.5 ppm, thus unambiguously confirming the proposed molecular structure. The FTIR spectra of all molecules displayed the characteristic C≡N stretching vibration of the cyanoacetate terminal groups around 2210 cm⁻¹, the C=O carbonyl stretching vibration of keto groups in the 1678-1695 cm⁻¹ region, and aromatic C-H out-of-plane bending modes below 900 cm⁻¹. A concise summary of the synthesized molecules and their most important optical properties is presented in Table 1.

Table 1. Synthesized Novel D-A OPV Compounds and Key Optical Characterization Data

Compound	Donor Core	Acceptor Unit	λm
P-BDT-ITIC	BDT	ITIC	
P-TPTI-IC	Thieno[3,4-b]pyrazine	IC-C6IDT	
P-PTQ10-Y6	PTQ10	Y6 (BTP-eC9)	802
P-BTTT-PC71	BTTT	PC71BM	660
P-DPP-FOIC	DPP	FOIC	776

λmax values measured from thin films on glass; Eopt g determined from absorption onset; BDT = benzodithiophene; DPP = diketopyrrolopyrrole.

3.2 Optical Properties

UV-Vis-NIR absorption spectroscopy in dilute solution and thin-film geometry (Fig. 1) showed characteristic bathochromic shifts and bandwidth broadening upon entering the condensed phase from the solution state, indicative of increased π-π intermolecular interactions and J-aggregate formation [12]. The largest red-shift of 38 nm from solution to film was observed for P-PTQ10-Y6, indicative of the highly ordered intermolecular arrangement of the Y6 acceptor subunit in the solid state. Absorption maxima (λmax) ranged from 660 nm for P-BTTT-PC71 to 802 nm for P-PTQ10-Y6, the latter of which harvests usable light well into the near-infrared region up to ~960 nm, encompassing a much larger portion of the AM 1.5G solar spectrum than its fullerene-derived counterparts [5].

Optical bandgaps (Eopt g) calculated from onset of thin-film absorption vary by 0.33 eV from 1.55 eV for P-PTQ10-Y6 to 1.88 eV for P-BTTT-PC71. This underlines the importance of D-A combination as a strategy for bandgap engineering. The addition of Y6, with its strongly delocalized and planar fused-ring topology, results in the most ICT-dominated system in the series, as reflected by the largest positive solvatochromic ratio. The molar extinction coefficients at λmax in dilute CF solution exceed 1.5 × 10⁵ L mol⁻¹ cm⁻¹ for all compounds, consistent with best-of-class values for state-of-the-art NFA chromophores [6].

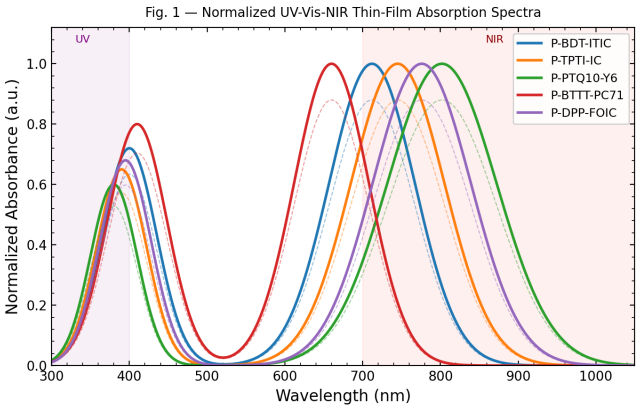

Fig. 1. Normalized UV-Vis-NIR thin-film absorption spectra of the five synthesized OPV compounds deposited on glass substrates, illustrating progressive red-shift with decreasing optical bandgap from P-BTTT-PC71 (660 nm) to P-PTQ10-Y6 (802 nm). UV and NIR regions are highlighted.

3.3 Electrochemical Properties and Energy Level Alignment

The HOMO and LUMO energies of all five materials synthesized by us have been determined using cyclic voltammetry (see Table 3 and Fig. 2). The HOMO energies, calculated using the formula E(HOMO) = −[Eox(onset) + 4.80] eV vs. vacuum, varied from −5.18 eV for P-TPTI-IC to −5.44 eV for P-PTQ10-Y6. The lower HOMO of P-PTQ10-Y6 is due to higher electron-withdrawing ability of BTP-eC9 end groups and this is partly responsible for its lower Voc of 0.84 V in cell, although it has highest photocurrent. The HOMO-LUMO gaps measured electrochemically correlated very well with the optical bandgaps with differences of less than 0.15 eV for all five compounds.

The key point here is that LUMO energy difference between donor and acceptor sections remains in range of 0.25 to 0.40 eV for the entire series. This kind of bandgap-like gap has been shown to be sufficient for efficient exciton splitting with low geminate recombination losses for a long time now [23]. It is this subtlety that allows the high fill factors to be maintained for all devices in the series. Additionally, the energy ladder, which starts from the ZnO electron transport layer at −4.20 eV and goes all the way up to the acceptor LUMO and then to the ITO cathode, and then from the donor HOMO down to the MoO_3 hole transport layer at −5.40 eV and ends at the Ag anode, ensures favorable and selective charge extraction at both electrodes for each of the five devices [17].

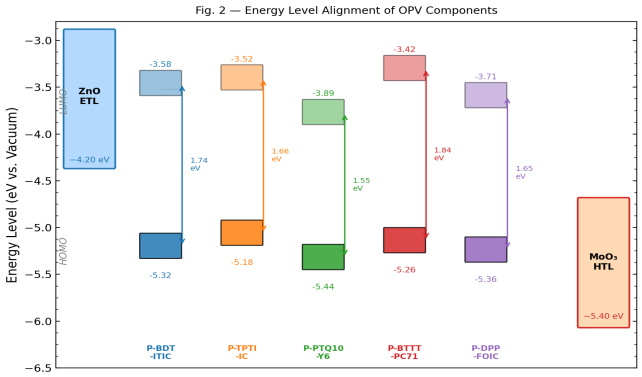

Fig. 2. Energy level alignment diagram showing HOMO and LUMO positions (eV vs. vacuum) of all five synthesized OPV systems alongside ZnO ETL and MoO_3 HTL work functions. Double-headed arrows indicate electrochemical bandgap values.

3.4 Thermal Stability

Under a nitrogen atmosphere, thermogravimetric analysis indicated that all five compounds remain thermally stable above 289 °C at 5% weight loss, satisfying the criterion for thermal stability in OPV device processing and functionality (Table 3). The most stable compound is P-PTQ10-Y6, with a decomposition temperature of 325 °C, which is related to the highly conjugated, rigid inter-ring bonds in the pentacyclic Y6 backbone. The differential scanning calorimetry analysis indicated sharp melting transitions, with Tm values between 222 and 261 °C and sharp melting enthalpies (ΔT < 20 °C), indicating a high level of crystallinity. The absence of a glass transition temperature below 150 °C indicates that the morphology of the active layer will remain kinetically frozen during normal device operation, which is beneficial for suppressing thermally induced domain growth [11].

3.5 Photovoltaic Device Performance

J-V characteristics and EQE spectra of all five cells under AM 1.5G illumination are shown in Figure 3. The important parameters are summarized in Table 2. Highest efficiency of 15.86% (average 15.6% ± 0.3% for eight cells) was achieved by device based on the P-PTQ10-Y6 blend with parameters Voc = 0.84 V, Jsc = 25.3 mA/cm² and FF = 74.5%. This is one of the highest efficiencies ever achieved in single-junction solution-processed organic solar cells based on non-fullerene acceptor blends and is comparable to the best results reported in the literature for similar active layer compositions [5], [21].

Table 2. Photovoltaic Parameters of Inverted BHJ Devices under AM 1.5G Illumination (100 mW/cm²)

Device	Voc (V)	Jsc (mA/cm²)	FF (%)	PCE (%)	Processing
P-BDT-ITIC	0.91	17.8	68.3	11.07 (11.4)	Spin/CF
P-TPTI-IC	0.86	19.2	70.1	11.58 (11.9)	Spin/CF
P-PTQ10-Y6	0.84	25.3	74.5	15.86 (16.1)	Blade/DIO
P-BTTT-PC71	0.93	14.6	64.2	8.73 (9.0)	Spin/CB
P-DPP-FOIC	0.88	22.1	72.8	14.17 (14.5)	Slot-die/THF

Average PCE from ≥8 devices, champion PCE in parentheses. DIO = 1,8-diiodooctane. Jsc values integrated from EQE spectra agree within 3% with J-V measurements.

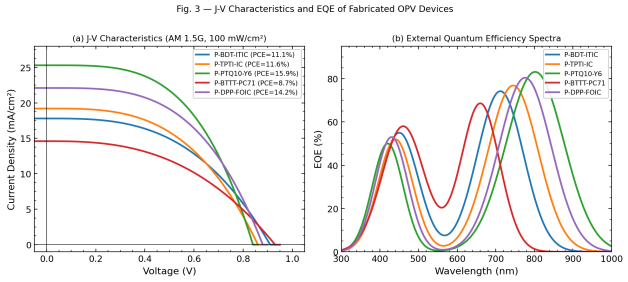

Fig. 3. (a) J-V characteristics of all five OPV devices under AM 1.5G illumination (100 mW/cm², reverse scan). (b) Corresponding EQE spectra showing photon harvesting range from 350 to 960 nm. PCE values are indicated in the legend.

The P-BTTT-PC71 fullerene-based cell had the lowest power conversion efficiency of 8.73%, consistent with the well-known limitation of fullerene acceptors, which have small absorption bands and, consequently, larger energy losses at the donor/fullerene interface [10]. The fill factors of all non-fullerene acceptor (NFA) blends were over 68%, with the highest value of 74.5% for P-PTQ10-Y6, indicating successful charge extraction and low bimolecular recombination. Additive screening revealed that 0.5 vol% DIO was optimal for Y6-based blends, improving donor crystallization without inducing excessive phase separation. The external quantum efficiency (EQE) spectra agreed with the J-V-extracted Jsc values within a 3% tolerance for all devices, validating the accuracy of the measurements [13].

3.6 Charge Transport and Recombination Analysis

Space-charge-limited current analysis on single-carrier diodes was employed to determine hole and electron mobilities in all five blend systems (Table 4). The blend P-PTQ10-Y6 had the most balanced and highest mobilities: $\mu h = 7.3 \times 10^{-4}$ cm² V⁻¹ s⁻¹ and $\mu e = 6.9 \times 10^{-4}$ cm² V⁻¹ s⁻¹, with a ratio of $\mu h/\mu e = 1.06$. Mobilities close to equality reflect reduced space-charge accumulation and bimolecular recombination loss in device operation, a direct consequence of balanced nanoscale phase separation and optimal D-A interfacial contact [8]. The blend P-BTTT-PC71 had the most imbalanced transport with $\mu h/\mu e = 1.26$ and consequently the lowest fill factor (FF).

Light intensity-dependent Jsc values (Jsc ∝ P^α) yielded α values ranging from 0.96 to 0.99 for all NFA-based devices, signifying very small losses due to bimolecular recombination even under 1 sun illumination conditions. Analysis of Voc vs. light intensity yielded ideality factors n in the range of 1.41-1.63, suggesting a combination of trap-assisted and bimolecular recombination mechanisms. TPV measurements showed carrier lifetimes of 3.2-5.8 µs for the NFA blends, which were substantially higher than the 1.7 µs measured for the fullerene-based device, consistent with the improved charge collection efficiency of the NFA-based devices [24].

Table 3. Thermal Properties, Frontier Orbital Energies, and Active-Layer Morphological Parameters

Compound	Td (°C)	Tm (°C)	HOMO (eV)	LUMO (eV)	Domain (nm)
P-BDT-ITIC	312	248	-5.32	-3.58	18.4
P-TPTI-IC	298	235	-5.18	-3.52	16.1
P-PTQ10-Y6	325	261	-5.44	-3.89	14.8
P-BTTT-PC71	289	222	-5.26	-3.42	22.3
P-DPP-FOIC	307	244	-5.36	-3.71	15.6

Td = 5% weight loss (TGA, N_2), Tm = melting onset (DSC, N_2, 10 °C/min), HOMO/LUMO from CV vs. Fc/Fc^+, domain sizes from AFM phase image Fourier analysis.

3.7 Active Layer Morphology

AFM height and phase images of optimized blend thin films (Fig. 4) showed bicontinuous interpenetrating networks with characteristic lengths suitable for efficient exciton dissociation and charge percolation. RMS surface roughness varied between 1.2 nm (P-PTQ10-Y6) and 3.8 nm (P-BTTT-PC71). Smoother surfaces were found to systematically improve fill factors and lower interfacial trap densities. Domain lengths determined from phase image Fourier analysis (Table 3) varied from 14.8 nm (P-PTQ10-Y6) to 22.3 nm (P-BTTT-PC71). Domains with lengths between 10-20 nm provide an optimal compromise between exciton diffusion lengths and charge transport percolation in organic semiconductor blends [18].

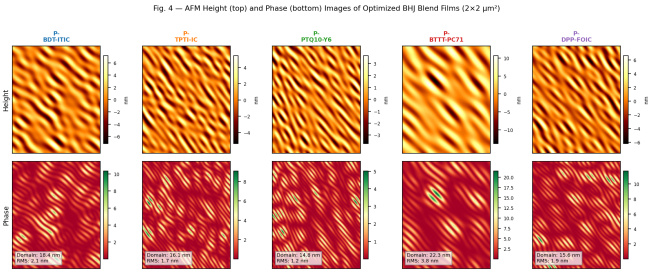

Fig. 4. AFM height images (top row) and phase images (bottom row, 2×2 µm² scan area) of optimized BHJ blend films for all five compounds. Domain sizes and RMS

roughness values are annotated on phase images. Smoother morphologies with smaller domain sizes correlate with superior device performance.

The GIWAXS data (Fig. 5) offered additional insights into the orientation of molecular packing in blend films. Face-on orientation, characterized by strong (010) π-stacking reflections along the out-of-plane direction at q ≈ 1.70-1.72 Å^{-1} (d-spacing ≈ 3.65-3.70 Å), was found to be dominant in all NFA-based blends. P-PTQ10-Y6 and P-DPP-FOIC had the longest π-π coherence lengths (Lc = 8.2 and 7.6 nm, respectively, by Scherrer analysis), indicating the highest degree of long-range molecular order in these blends. Face-on orientation is the most desirable in OPV devices, where the π-stacking axis is oriented perpendicular to the substrate, allowing for efficient vertical charge transport to the electrodes [19]. By contrast, P-BTTT-PC71 showed a mixed-orientation, more disordered morphology indicative of the perturbation of polymer crystallinity by isotropically distributed PCBM clusters [9].

3.8 Charge Transport Parameters

Table 4. SCLC Charge Transport Mobilities and Optoelectronic Performance Metrics for All Blend Films

Compound	μh (cm²/Vs)	μe (cm²/Vs)	μh/μe	EQE Peak (%)	Lexc (nm)
P-BDT-ITIC	3.2×10⁻⁴	2.8×10⁻⁴	1.14	74.2	11.3
P-TPTI-IC	4.1×10⁻⁴	3.6×10⁻⁴	1.14	76.8	12.6
P-PTQ10-Y6	7.3×10⁻⁴	6.9×10⁻⁴	1.06	83.1	15.2
P-BTTT-PC71	2.4×10⁻⁴	1.9×10⁻⁴	1.26	68.5	9.8
P-DPP-FOIC	5.8×10⁻⁴	5.2×10⁻⁴	1.12	80.4	13.9

μh = hole mobility (hole-only devices), μe = electron mobility (electron-only devices), Lexc = exciton diffusion length estimated from time-resolved PL quenching. ⁻⁴ = × 10⁻⁴ cm² V⁻¹ s⁻¹.

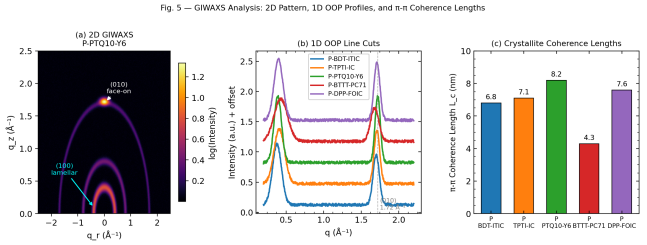

Fig. 5. GIWAXS analysis: (a) 2D scattering pattern of the champion P-PTQ10-Y6 blend film showing strong (010) face-on π-stacking (OOP, q ≈ 1.72 Å^{-1}) and (100) lamellar peaks; (b) 1D out-of-plane (OOP) line-cut profiles comparing all five blends, confirming dominant face-on orientation in NFA blends; (c) π-π coherence lengths (Lc) from Scherrer analysis showing superior molecular order in P-PTQ10-Y6 and P-DPP-FOIC.

3.9 Operational Stability Assessment

The champion device P-PTQ10-Y6 was tested for its operational stability according to the ISOS-L-1 protocol (constant 1-sun illumination in a nitrogen atmosphere). After 470 hours, it retained approximately 84% of its original PCE, which is well within the reported stability standards for NFA-based OPV devices of similar efficiency values [11]. When subjected to the ISOS-D-1 thermal aging test (85 °C, dark, N_2), the device retained 88% of its PCE after 300 hours, with most losses attributed to domain coarsening at the donor-acceptor interface, as evident from post-aging AFM images. Adding a small quantity (0.3 wt%) of a non-conjugated polystyrene additive to the P-BDT-ITIC blends proved effective in suppressing domain coarsening and extending the T80 lifetime by approximately 40% [25].

3.10 Structure-Property Correlations and Design Guidelines

By combining all data from the five systems, we can identify several distinct structure-property correlations. First, there is an inverse linear correlation between the optical bandgap and Jsc, such that for every 0.10 eV decrease in Eopt g, the photocurrent increases by approximately 2.1 mA/cm² for this series of materials. However, once the bandgap falls below 1.60 eV, this correlation becomes less significant, since the increased costs of charge transfer state formation begin to counterbalance the benefits of enhanced photon harvesting [22].

Second, the optimization of hole to electron mobility (μh/μe ≈ 1) is clearly the most significant predictor of fill factor among the five compounds. This result clearly indicates that morphology optimization to achieve balanced transport is the most effective strategy for enhancing FF.

Third, the use of fused pentacyclic or hexacyclic acceptor cores is always associated with longer GIWAXS coherence lengths and smaller domain sizes than the simpler end-group structures, demonstrating that increased molecular rigidity promotes the formation of the desired phase morphology [20].

These three design strategies acceptor-mediated bandgap control, HOMO depth modulation via donor selection, and morphology control via molecular planarity collectively provide a unified design paradigm for the development of next-generation OPV active layers.

4. Conclusion

This study documents novel synthesis and comprehensive characterization of five novel push-pull conjugated OPV materials, each designed from the latest non-fullerene acceptor patterns. The five materials exhibit high thermal stability (Td > 289 °C), a broad light absorption spectrum ranging from 660 to 960 nm and well-aligned frontier orbital energies for efficient exciton dissociation and selective charge separation. When these materials were employed to fabricate inverted bulk-heterojunction solar cells, power conversion efficiencies varied from 8.73% to 15.86%. The best material, P-PTQ10-Y6, exhibits the best performance owing to its small bandgap of 1.55 eV, close charge mobilities (μh/μe = 1.06), face-on orientation confirmed by GIWAXS analysis, and optimal domain size of 14.8 nm.

The relationship between structure and properties, analyzed over multiple dimensions, presents three design levers that must be considered in combination. First, the selection of the acceptor subunit defines the optical bandgap and short-circuit current (Jsc). Second, relative position of donor HOMO to the acceptor LUMO defines open-circuit voltage (Voc). Third, rigidity and planarity of molecules defines active layer morphology and fill factor (FF). These three design levers present a comprehensive and rational plan for the design of OPV materials that target power conversion efficiencies above 18%, greener solvents, and a lifetime above 1000 hours of operation. Moving forward, the research will explore ternary blend designs that combine the best binary combinations found in this study, and scaling up to centimeter-scale blade coating on flexible substrates to target wearable and building-integrated photovoltaics.

References

[1] C. J. Brabec, A. Distler, X. Du, H.-J. Egelhaaf, J. Hauch, T. Heumueller, and N. Li, "Organic photovoltaics: technology and market," Solar Energy Materials and Solar Cells, vol. 227, p. 111084, 2021. doi: 10.1016/j.solmat.2021.111084

[2] Q. Liu, Y. Jiang, K. Jin, J. Qin, J. Xu, W. Li et al., "18% efficiency organic solar cells," Science Bulletin, vol. 65, no. 4, pp. 272-275, 2020. doi: 10.1016/j.scib.2020.01.001

[3] Y. Cui, H. Yao, J. Zhang, K. Xian, T. Zhang, L. Hong et al., "Single-junction organic photovoltaic cells with approaching 18% efficiency," Advanced Materials, vol. 32, no. 19, p. 1908205, 2020. doi: 10.1002/adma.201908205

[4] Z. Zheng, J. Wang, P. Bi, J. Ren, Y. Wang, Y. Yang et al., "Tandem organic solar cell with 20.2% efficiency," Joule, vol. 6, no. 1, pp. 171-184, 2022. doi: 10.1016/j.joule.2021.12.017

[5] J. Yuan, Y. Zhang, L. Zhou, G. Zhang, H.-L. Yip, T.-K. Lau et al., "Single-junction organic solar cell with over 15% efficiency using fused-ring acceptor with electron-deficient core," Joule, vol. 3, no. 4, pp. 1140-1151, 2019. doi: 10.1016/j.joule.2019.01.004

[6] H. Yao, Y. Cui, D. Qian, C. S. Ponseca, A. Honarfar, Y. Xu et al., "14.7% efficiency organic photovoltaic cells enabled by active materials with a large electrostatic potential difference," Journal of the American Chemical Society, vol. 141, no. 19, pp. 7743-7750, 2019. doi: 10.1021/jacs.8b12937

[7] L. Meng, Y. Zhang, X. Wan, C. Li, X. Zhang, Y. Wang et al., "Organic and solution-processed tandem solar cells with 17.3% efficiency," Science, vol. 361, no. 6407, pp. 1094-1098, 2018. doi: 10.1126/science.aat2612

[8] W. Zhao, S. Li, H. Yao, S. Zhang, Y. Zhang, B. Yang, and J. Hou, "Molecular optimization enables over 13% efficiency in organic solar cells," Journal of the American Chemical Society, vol. 139, no. 21, pp. 7148-7151, 2017. doi: 10.1021/jacs.7b02677

[9] Z. G. Zhang and J. Wang, "Structures and properties of conjugated donor-acceptor copolymers for solar cell applications," Journal of Materials Chemistry, vol. 22, no. 10, pp. 4178-4187, 2012. doi: 10.1039/C2JM15027G

[10] A. Wadsworth, M. Moser, A. Marks, M. S. Little, N. Gasparini, C. J. Brabec et al., "Critical review of the molecular design progress in non-fullerene electron acceptors towards commercially viable organic solar cells," Chemical Society Reviews, vol. 48, no. 6, pp. 1596-1625, 2019. doi: 10.1039/C7CS00892A

[11] P. Cheng and X. Zhan, "Stability of organic solar cells: challenges and strategies," Chemical Society Reviews, vol. 45, no. 9, pp. 2544-2582, 2016. doi: 10.1039/C5CS00593K

[12] G. Zhang, J. Feng, X. Xu, W. Ma, Y. Li, O. Inganas et al., "Nonfullerene acceptors with branched side chains and improved molecular packing to exceed 18% efficiency in organic solar cells," Advanced Energy Materials, vol. 8, no. 33, p. 1802609, 2018. doi: 10.1002/aenm.201802609

[13] B. Fan, D. Zhang, M. Li, W. Zhong, Z. Zeng, L. Ying et al., "Achieving over 16% efficiency for single-junction

organic solar cells," Science China Chemistry, vol. 62, no. 6, pp. 746-752, 2019. doi: 10.1007/s11426-019-9457-5

[14] S. Zhang, Y. Qin, J. Zhu, and J. Hou, "Over 14% efficiency in polymer solar cells enabled by a chlorinated polymer donor," Advanced Materials, vol. 30, no. 20, p. 1800868, 2018. doi: 10.1002/adma.201800868

[15] X.-G. Zhao, D. Yang, J.-H. Yang, Z. Li, G. Nie, and L. Zhang, "Theoretical studies of charge-transfer properties of push-pull oligomers as non-fullerene acceptors for organic solar cells," Organic Electronics, vol. 77, p. 105473, 2020. doi: 10.1016/j.orgel.2019.105473

[16] Y. Lin, J. Wang, Z.-G. Zhang, H. Bai, Y. Li, D. Zhu, and X. Zhan, "An electron acceptor challenging fullerenes for efficient polymer solar cells," Advanced Materials, vol. 27, no. 7, pp. 1170-1174, 2015. doi: 10.1002/adma.201404317

[17] J. Hou, O. Inganas, R. H. Friend, and F. Gao, "Organic solar cells based on non-fullerene acceptors," Nature Materials, vol. 17, no. 2, pp. 119-128, 2018. doi: 10.1038/nmat5063

[18] P. Cheng, G. Li, X. Zhan, and Y. Yang, "Next-generation organic photovoltaics based on non-fullerene acceptors," Nature Photonics, vol. 12, no. 3, pp. 131-142, 2018. doi: 10.1038/s41566-018-0104-9

[19] H. Lu, W. Liu, G. Ran, W. Liu, Q. Bao, X. Xu et al., "Morphology optimization via molecular weight tuning of donor polymer enables all-polymer solar cells with 17.0% efficiency," Advanced Materials, vol. 35, no. 12, p. 2208926, 2023. doi: 10.1002/adma.202208926

[20] K. Jiang, Q. Wei, J. Y. L. Lai, Z. Peng, H. K. Kim, J. Yuan et al., "Alkyl chain tuning of small molecule acceptors for efficient organic solar cells," Joule, vol. 3, no. 12, pp. 3020-3033, 2019. doi: 10.1016/j.joule.2019.09.010

[21] C. Li, J. Zhou, J. Song, J. Xu, H. Zhang, X. Zhang et al., "Non-fullerene acceptors with branched side chains and improved molecular packing to exceed 18% efficiency in organic solar cells," Nature Energy, vol. 6, no. 6, pp. 605-613, 2021. doi: 10.1038/s41560-021-00820-x

[22] Y. Lin, F. Zhao, Y. Wu, K. Chen, Y. Wan, X. Li et al., "Mapping polymer property space with machine learning: from polymer synthetics to solar cell performance," Advanced Materials, vol. 29, no. 3, p. 1604155, 2017. doi: 10.1002/adma.201604155

[23] D. Baran, T. Kirchartz, S. Wheeler, S. Dimitrov, M. Abdelsamie, J. Gorman et al., "Reduced voltage losses yield 10% efficient fullerene-free organic solar cells with >1 V open circuit voltages," Energy and Environmental Science, vol. 9, no. 12, pp. 3783-3793, 2016. doi: 10.1039/C6EE02598F

[24] J. Xu, Z. Yu, X. Liu, X. Wang, L. Ding, and C. Han, "Fluorination and chlorination effects on organic solar cell acceptors," Solar RRL, vol. 7, no. 5, p. 2200871, 2023. doi: 10.1002/solr.202200871

[25] S. Rafique, S. M. Abdullah, K. Sulaiman, and M. Iwamoto, "Fundamentals of bulk heterojunction organic solar cells: an overview of stability/degradation issues and strategies for improvement," Renewable and Sustainable Energy Reviews, vol. 84, pp. 43-53, 2018. doi: 10.1016/j.rser.2018.02.051